Uncertainty Analysis of NO Production During Methane Combustion

I. GY. ZSÉLY, J. ZÁDOR, T. TURÁNYI

Laboratory for Chemical Kinetics, Institute of Chemistry, Eötvös University (ELTE), *Budapest, Hungary*

Received 27 November 2007; revised 19 April 2008, 31 May 2008; accepted 31 May 2008

DOI 10.1002/kin.20373
Published online in Wiley InterScience (www.interscience.wiley.com).

ABSTRACT: Local and Monte Carlo uncertainty analyses of NO production during methane combustion were carried out, investigating the effect of uncertainties of kinetic parameters and enthalpies of formation. In Case I, the original Leeds methane oxidation mechanism with the NO_x reaction block was used, but the enthalpies of formation of all species were updated. In Case II, the NCN-containing reactions of the prompt NO formation route were added and the rate parameters of several reactions were also updated. The NO production was examined at the conditions of the Bartok et al. experiments (PSR, T = 1565–1989 K, $\varphi = 0.8$–1.2, residence time 3 ms). The Monte Carlo analysis provided the approximate probability density function and the variance of the calculated NO concentration, and also its attainable minimum and maximum values. Both mechanisms provided similarly good to acceptable agreement with the experimental results for lean and stoichiometric mixtures, whereas only mechanism Case II could reproduce the experimental data for rich mixtures after a realistic tuning of the parameters. Local uncertainty analysis was used to assess the contribution of the uncertainty of each parameter to the uncertainty of the calculated NO concentration. Enthalpies of formation of NNH and HCCO, and rate parameters of 20 reaction steps cause most of the uncertainty of the calculated NO concentrations at all conditions. The relative importance of the four main NO formation routes was investigated via the inspection of the reaction rates, embedded in the Monte Carlo analysis. NO formation in rich mixtures was dominated by the prompt route, whereas in leaner mixtures the share of the NO formation routes depended very much on the values of rate parameters, when varied within the uncertainty limits of kinetic data evaluations.
 Int J Chem Kinet 40: 754–768, 2008

INTRODUCTION

Detailed reaction mechanisms are widely used in various fields, such as combustion, pyrolysis, atmospheric chemistry, and so on, and the proposed mechanisms have been tested against measurement data. Usually, there is not a prefect coincidence between the measured and the simulated data, and the level of agreement can be judged only by knowing both the measurement error and uncertainty of simulation results. Although there is a well-established practice of the assessment of measurement error, investigation of the uncertainty of simulation results of chemical kinetic models received more attention only recently.

Uncertainty analysis of atmospheric chemical and air quality models has been carried out for several decades. There are fewer examples for the application

Correspondence to: T. Turányi; e-mail: turanyi@chem.elte.hu.
Present address of J. Zádor: Combustion Research Facility, Sandia National Laboratories, Livermore, CA.
Contract grant sponsor: OTKA.
Contract grant number: T68256.

of uncertainty analysis in the investigation of combustion chemical models [1–11]. Warnatz [1], Bromly et al. [2], Brown et al. [3], and Turányi et al. [4] have calculated uncertainties based on local sensitivity coefficients. Global methods require much more powerful computational resources, but can take into account the whole range of parameter uncertainties. In the literature of combustion, global methods were used by Phenix et al. [5], Reagan et al. [6], Zádor et al. [7,8], Zsély et al. [9], and Tomlin and coworkers [10,11]. None of these articles dealt with the NO production in methane combustion, although this is one of the central problems in combustion chemistry. Tomlin and coworkers [10,11] investigated the interaction of sulfur and nitrogen species in methane flames. Nitric oxide is a major air pollutant, and almost all emitted NO comes from combustion processes. Design of industrial furnaces with low NO emission is a foremost aim. Computer aided design of combustors requires the prediction of NO concentration, which is not imaginable without good understanding of the background chemistry. This paper presents the investigation of the reliability of NO concentration calculations in the simulation of perfectly stirred reactor experiments and the share of the main NO formation routes.

UNCERTAINTY ANALYSIS

A detailed methodology for the consideration of the uncertainties of kinetic and thermodynamic parameters on the simulation results of gas kinetic systems based on local uncertainty analysis has been described in our previous paper [4]. This technique was recently extended to the application of global uncertainty analysis [7]. Here, a brief summary is given, which focuses on the methods used in this paper.

Critical compilations of gas kinetic rate parameters (see, e.g., [12–18]) provide not only the recommended kinetic parameters, but also report the accuracy of the data by assigning an uncertainty factor to them. This uncertainty factor f_j has been defined in the following way:

$$f_j = \log_{10}\left(\frac{k_j^0}{k_j^{\min}}\right) = \log_{10}\left(\frac{k_j^{\max}}{k_j^0}\right) \qquad (1)$$

where k_j^0 is the recommended value of the rate coefficient of reaction j, and $k_j^{\min}$ and $k_j^{\max}$ are the extreme values; rate coefficients outside the $[k_j^{\min}, k_j^{\max}]$ interval are considered physically nonrealistic by the evaluators. Assuming that the minimum and maximum values of rate parameters correspond to 3σ deviations from the recommended values on a logarithmic scale [19], the uncertainty factor can be converted [4] to the variance of the logarithm of the rate coefficient using the equation $\sigma^2(\ln k_j) = ((f_j \ln 10)/3)^2$.

Thermodynamic data compilations of gas kinetic modeling relevance [20–31] contain not only the enthalpy of formation of the species but also frequently quote their uncertainty. This uncertainty corresponds to 2σ. The quoted uncertainty of the enthalpies of formation was transformed to 1σ standard deviation in this paper. Also, we did not consider the enthalpy of formation values outside the $\pm 3\sigma$ limits.

In this paper and in all previous works that dealt with uncertainty analysis of combustion chemical systems, thermodynamic and kinetic parameters were assumed to be uncorrelated. Thermodynamic tables and kinetic data evaluations contain data on the uncertainty of each parameter separately, and there is no information on the correlation of them. The Active Table approach of Ruscic et al. [31–33] provides a set of recommended enthalpies of formation and also their correlation matrix or even their joint probability density function (PDF). Similar correlation information could be obtained for the rate parameters from the kind of calculations that were published by Frenklach et al. [34,35]. However, currently no correlation information is available for the enthalpies of formation of species and kinetic parameters of reactions related to the NO formation during methane combustion.

Application of global methods requires not only the mean and the variance of the parameters but also their PDFs. In the lack of more detailed information and based on the central limit theorem, normal distribution was assumed for parameters $\ln k$ and ΔH_f^θ (298.15 K), truncated at $\pm 3\sigma$. This means that the minimum and maximum values of these parameters were $p_j^0 - 3\sigma(p_j)$ and $p_j^0 + 3\sigma(p_j)$, respectively, and parameter values outside these limits were considered as physically not realistic.

According to linear uncertainty analysis, assuming that the rate coefficients are not correlated, the variance of model output Y_i can be calculated in the following way:

$$\sigma_{K_j}^2(Y_i) = \left(\frac{\partial Y_i}{\partial \ln k_j}\right)^2 \sigma^2(\ln k_j) \qquad (2)$$

$$\sigma_K^2(Y_i) = \sum_j \sigma_{Kj}^2(Y_i) \qquad (3)$$

In these equations, subscript K refers to an uncertainty of kinetic origin, $\sigma^2(\ln k_j)$ is the variance of the logarithm of rate coefficient k_j, and $(\partial Y_i/\partial \ln k_j)^2$ is the square of the seminormalized local sensitivity

coefficient. Partial variance $\sigma^2_{K_j}(Y_i)$ is the contribution of the uncertainty of the rate coefficient of reaction j to the variance of model output Y_i.

The influence of the enthalpy of formation data on the model result can be calculated in a similar way, assuming that the data are uncorrelated:

$$\sigma^2_{\mathrm{T}\,j}(Y_i) = \left(\frac{\partial Y_i}{\partial \Delta H^\theta_f(j)}\right)^2 \sigma^2\left(\Delta H^\theta_f(j)\right) \qquad (4)$$

$$\sigma^2_{\mathrm{T}}(Y_i) = \sum_j \sigma^2_{\mathrm{T}j}(Y_i) \qquad (5)$$

where subscript T refers to thermodynamic uncertainty; $\partial Y_i/\partial \Delta H^\theta_f(j)$ is the local enthalpy of formation sensitivity coefficient, which is a linear estimation of the effect of changing the enthalpy of formation; $\sigma^2_{\mathrm{T}}(Y_i)$ is the variance of model output Y_i due to the uncertainties of the enthalpies of formation of all species. Partial thermodynamic uncertainty contribution $\sigma^2_{\mathrm{T}\,j}(Y_i)$ is the contribution of the uncertainty of the enthalpy of formation of species j to the variance of model output Y_i. The sum of the variances of kinetic and thermodynamic origin provides the variance of model result:

$$\sigma^2(Y_i) = \sigma^2_{\mathrm{K}}(Y_i) + \sigma^2_{\mathrm{T}}(Y_i) \qquad (6)$$

We can also calculate values

$$S\%_{ij} = \frac{\sigma^2_j(Y_i)}{\sigma^2(Y_i)} \times 100 \qquad (7)$$

where $\sigma^2_j(Y_i)$ is either of kinetic or thermodynamic origin. This shows the percentage contribution of a parameter to the uncertainty of model output Y_i.

Most of the simulation programs in chemical kinetics include built-in routines to calculate local sensitivity coefficients; therefore, the variances and uncertainty contributions above can be easily calculated. The drawback of this method is that the calculated values are local estimates only, and the accuracy of this approximation cannot be assessed.

In the Monte Carlo analysis (see, e.g., [36]), a large number of parameter sets are generated according to the PDFs of the parameters. The model is simulated with each of these parameter sets, and the results are processed with statistical methods. Application of Latin hypercube sampling (LHS) [36] allows computationally efficient, but unbiased Monte Carlo simulations. In LHS, the ranges of parameters are divided into intervals of equal probability. The parameter values are randomly and independently sampled in each interval, and the selected values of the parameters are randomly grouped without repetition. This way, all parameters are changed simultaneously and the parameter sets cover the whole available parameter space. Therefore, the minimum and maximum values collected from the Monte Carlo analysis results provide a good estimate of the attainable minimum and maximum model results. If the experimental data lie outside the range of attainable results, then the structure of the model is surely wrong (e.g., important reactions are missing), provided that the PDFs of the parameters have been estimated correctly and the experimental data are accurate.

NO FORMATION IN COMBUSTION SYSTEMS

In methane combustion systems, NO can be formed in four routes (see, e.g., [37]). At high temperature, NO is formed in the *thermal route*:

$$\mathrm{N_2 + O = N + NO} \qquad \text{(R1)}$$

The N-atom produced reacts further in reactions $\mathrm{N + O_2 = NO + O}$ and $\mathrm{N + OH = NO + H}$.

When the CH concentration is high, the *prompt NO formation* is significant.

$$\mathrm{N_2 + CH = HCN + N} \qquad \text{(R2a)}$$

For decades, reaction (R2a) was considered as the main initiation step of the prompt NO route, but Moskaleva and Lin [38] debated this reaction, and Smith gave an experimental evidence of NCN as an intermediate of the prompt-NO formation [39].

$$\mathrm{N_2 + CH = NCN + H} \qquad \text{(R2b)}$$

El Bakali et al. [40] included this prompt NO formation pathway to the GDF-Kin 3.0 reaction mechanism. Recently, Hanson and coworkers [41] studied the reaction between CH and N_2 in shock tube experiments using CH and NCN laser absorption. The CH measurements established NCN and H as the primary products of the $\mathrm{CH + N_2}$ reaction. These results were confirmed by Harding et al. [42], who investigated the potential energy surface for the $\mathrm{CH + N_2}$ reaction with multireference ab initio electronic structure methods. In the cases of both steps ((R2a) and (R2b)), the intermediate formed (HCN or NCN) is converted to NO through several steps.

The N_2O intermediate can be formed in the following steps, providing a via N_2O formation route of

NO:

$$N_2 + O(+M) = N_2O(+ M) \quad (R3)$$

$$N_2 + OH(+ M) = N_2O + H(+M) \quad (R4)$$

$$N_2 + HO_2(+ M) = N_2O + OH(+M) \quad (R5)$$

$$N_2 + O_2(+M) = N_2O + O(+ M) \quad (R6)$$

The N_2O formed is then mainly converted to NO in several steps.

The fourth way for the generation of NO is initiated by the reaction of N_2 with hydrocarbon-free species other than O. These species include H, OH, H_2, and H_2O. This is called the via NNH formation route of NO. The possible initiation reactions are the following:

$$N_2 + H = NH + N \quad (R7)$$

$$N_2 + OH = NH + NO \quad (R8)$$

$$N_2 + H = NNH \quad (R9)$$

$$N_2 + OH = NNH + O \quad (R10)$$

$$N_2 + H_2 = NNH + H \quad (R11)$$

$$N_2 + H_2O = NNH + OH \quad (R12)$$

The NNH produced is also converted mainly to NO.

In this paper, the investigations are based on the Leeds methane oxidation mechanism [43] with the NO_x reaction block extension [44]. The published works of Hughes et al. [43,44] contain results of comprehensive testing of the mechanism against experimental data. Two different versions of the Leeds mechanism were used. The mechanism used in Case I is identical to the Leeds methane oxidation mechanism with the NO_x block, but the enthalpies of formation of all species were revised and updated. The revised values for the C/H/O species have been published in [4] and [7], whereas the revised enthalpies of formation of nitrogen-containing species are given in Table I. To use a consistent set of data, in most cases the values recommended by Burcat [29] were applied.

This paper investigates the NO formation during methane combustion, so the complete neglect of the possible role of NCN in the prompt route could be criticized. For this reason, similarly to the paper of El Bakali et al. [40], we created a modified version of the Leeds mechanism (Case II): the debated reaction (R2a) was replaced with reaction (R2b) and NCN reactions were added (see Table II). In Case II, the highest sensitivity N-species reactions were identified and the rate coefficients of these reactions were updated. Table II contains also the updated reactions. This mechanism has not been comprehensively tested and cannot be considered as an updated version of the NO_x block of the Leeds methane oxidation mechanism.

Table I Enthalpies of Formation of the N-Containing Species and Their Standard Deviation

Species	ΔH_f^θ (298.15 K) kJ mol^{-1}	1σ standard deviation of ΔH_f^θ (298.15 K)[a] kJ mol^{-1}	Reference
CN	438.807[b]	0.26[b]	[29]
HCN	129.799[b]	0.19[b]	[29]
N	472.459[b]	0.02[b]	[29]
NH	358.78[b]	0.185[b]	[29]
NO	91.097[b]	0.043[b]	[33]
HNO	106.842[b]	0.0625[b]	[29]
NH_2	186.422[b]	0.10[b]	[58]
H_2NO	66.184	4.25	[59]
NCO	128.04	2.1	[29]
N_2O	82.58[b]	0.05[b]	[29]
NO_2	34.025[b]	0.043[b]	[33]
N_2H_2	211.859	5.0	[29]
HOCN	−15.456	10.0	[29]
H_2CN	240.162	5.0[c]	[29]
NNH	251.776	4.0	[29]
NH_3	−45.567[b]	0.015[b]	[29]
N_2H_3	220.58[b]	0.67[b]	[29]
C_2N_2	309.28[b]	0.52[b]	[29]
HNCO	−118.6	2.1	[29]
NCN	465.89[b]	0.89[b]	[29]

[a] Derived by halving the reported 95% confidence interval.
[b] The value was determined by the ATcT method [32].
[c] Estimated value (see text).

The Leeds methane oxidation mechanism has been utilized [4,7] for uncertainty studies. In this work, the same uncertainty factors were used to the kinetic and thermodynamic parameters of N-atom-free reactions and species, respectively, as in our former articles [4,7]. As a first step in the extension of these studies to NO_x systems, uncertainties had to be assigned to the enthalpies of formation of all N-containing species by processing thermodynamic data collections [12,14–17,20–29]. In most cases, the variances recommended in the databases were in agreement. Table I contains also the variances of the enthalpies of formation of the N-containing species. Some of the enthalpies of formation are based on active table calculations (see the footnote in Table I), but the quoted uncertainties refer to each species separately. No recommended uncertainty was found for the enthalpy of formation of H_2CN, and the quoted uncertainty value is estimated.

Based on kinetic data evaluations, uncertainty factors f_j were also assigned to the rate coefficients of N-containing reactions. All reaction steps in the mechanism are reversible; therefore, altered enthalpies of

Table II Added Reactions and Updated Rate Coefficients of N-Chemistry in Case II

Reaction Step	A	n	E	f	Reference
$N_2 + CH = NCN + H$	5.11E + 12	0.00	56.90	1.0[a]	[40]
$CN + N_2O = NCN + NO$	3.84E + 03	2.60	15.46	0.3	[60]
$CN + NCO = NCN + CO$	1.80E + 13	0.00	0.00	1.0[a]	[61]
$NCN + H = HCN + N$	1.00E + 14	0.00	0.00	1.0[a]	[61]
$NCN + O = CN + NO$	1.00E + 14	0.00	0.00	1.0[a]	[61]
$NCN + OH = HCN + NO$	5.00E + 13	0.00	0.00	1.0[a]	[61]
$NCN + O_2 = NO + NCO$	1.00E + 13	0.00	0.00	1.0[a]	[61]
$NO + NH = N_2 + OH$	6.86E + 14	−0.78	0.33	0.5	[18]
$NO + NH = N_2O + H$	2.75E + 15	−0.78	0.33	0.5	[18]
$NO_2 + H = NO + OH$	2.53E + 14	0.00	2.82	0.3	[18]
$HCN + OH = CN + H_2O$	3.91E + 06	1.83	43.07	0.5	[18]
$O + NNH = NH + NO$	4.45E + 14	0.00	87.63	0.5	[18]
$O + NCO = NO + CO$	4.33E + 13	0.00	0.00	0.3	[18]
$NO_2 + O = NO + O_2$	3.92E + 12	0.00	1.00	0.7[a]	[13]
$CH_3 + N = H_2CN + H$	7.10E + 14	0.00	0.00	0.5	[62]

Units are mol, cm^3, and kJ.
[a]Estimated uncertainty factors.

formation also changed the calculated rates of backward reactions.

For the simulations, the PSR code [45] of the CHEMKIN-II package [46] was used. The code was modified to allow the sequential calculations with many parameter sets for the Monte Carlo simulations and for the calculation of the local sensitivity coefficients of the enthalpies of formation. The local sensitivities were converted to uncertainty features using program KINALC [47]. Generation of Latin hypercube samples and analysis of Monte Carlo results were carried out using purpose written Fortran codes. Three Monte Carlo analyses were accomplished, and the number of simulations was increased in steps 1000, 3162, and 10,000. The averages and standard deviations did not change significantly from 1000 to 10,000 strata. The results presented in this paper correspond to 10,000 runs for each equivalence ratio and case.

UNCERTAINTY ANALYSIS OF THE NO_X MECHANISM

A generally used benchmark experiment for NO formation during methane combustion was made by Bartok et al. [48]. In this series of experiments, methane and air was preheated to the desired inlet temperature and premixed. The mixture was injected into a spherical jet-stirred reactor, which was designed to be close to a perfectly stirred reactor (PSR). The temperature was varied between 1565 and 1989 K. Equivalence ratio φ and residence time τ were changed from 0.6 to 1.6 and 1.2 to 3.0 ms, respectively. Atmospheric pressure was kept in the reactor. Table III contains the equivalence ratios and the corresponding gas temperatures of the experiments. The residence time was 3 ms in all simulated cases.

Table III Equivalence Ratios and the Corresponding Gas Temperatures of the Bartok et al. Experiments Simulated in This Paper

Equivalence Ratio	Temperature (K)
0.67	1565
0.76	1802
0.89	1874
0.935	1896
1.06	1989
1.205	1977
1.30	1937
1.54	1869
1.75	1809

Pressure was always 1 atm and the residence time was 3 ms.

The reason of the reputation of the Bartok et al. series of experiments [48] is that the applied domain of pressure, temperature, residence time, and equivalence ratio is close to the conditions of an industrial furnace. This experiment is widely used (see, e.g., publications [44,49,50]) for testing mechanisms of NO formation during methane oxidation.

In all figures in this paper, the results are presented using the Case I and Case II mechanisms in parallel. Figure 1 shows the measured outlet NO concentration (solid dots) as a function of the equivalence ratio and the corresponding measurement error (vertical lines) estimated on the basis of the work of

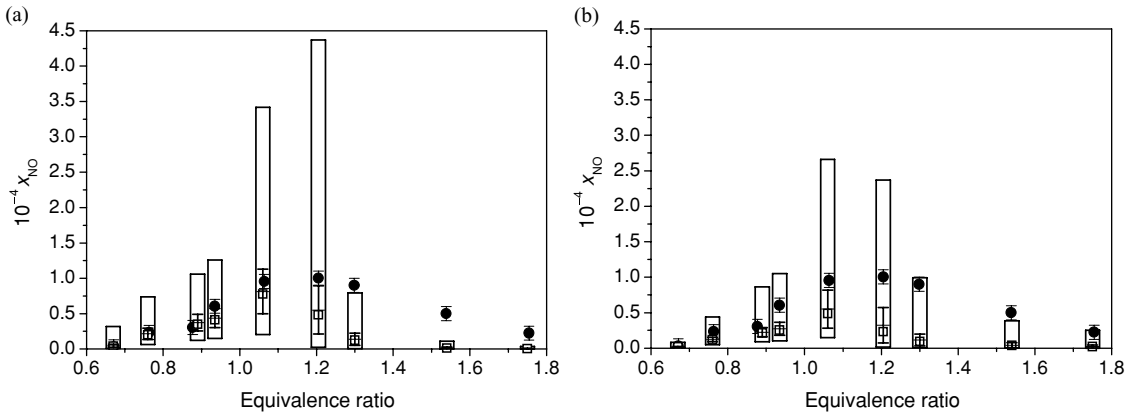

Figure 1 Results at the conditions of the Bartok et al. experiments, indicating the measured data (solid dots), the simulation results (empty squares), the 1σ error limits of the experimental and simulation data (vertical lines), and the limits of simulation results by tuning all parameters simultaneously within their physically realistic limits (boxes); (a) in Case I and (b) in Case II.

Bartok et al. [48]. This 1σ uncertainty reflects the error of the chemical analysis only, and possible systematic errors are not included. The simulated concentrations (empty squares) are in fair agreement with the measured data at lean compositions in both cases. The agreement is getting worse with increasing equivalence ratio, and the simulated concentrations underpredict the measured NO concentration. Note that the GRI 2.11 mechanism provided a good agreement [44,49,50] with the Bartok et al. data, but the latter 3.0 version [50] strongly overpredicted the NO concentration.

Monte Carlo analysis is an accurate method for the determination of the uncertainty of model results. Figure 1 shows the 1σ standard deviation of NO concentration as vertical lines determined by the Monte Carlo analysis. If equivalence ratio φ is less than 1.1, the 1σ standard deviation of the experimental and simulation results overlap in both cases. At large equivalence ratios, the experimental points are outside the 1σ standard deviation of the simulation results.

Tuning all parameters simultaneously within their physically realistic limits, minimum and maximum values of the results at physically realistic parameter combinations can be obtained, and these limits, shown as boxes in Fig. 1, can also be acquired from the Monte Carlo results. In Case I, at equivalence ratio $\varphi = 1.2$ and at leaner mixtures, the experimental points are within these boxes. This means that keeping the present set of elementary reactions and changing the parameters within the realistic limits, the experimental points could be reproduced. At equivalence ratios $\varphi = 1.3$ or higher, the experimental data cannot be reproduced using the current set of reaction steps. In Case II the situation is much better. For all fuel-to-air ratios, the experimental points are within (or close to) these limits, showing that the experimental points could be obtained by an optimized set of parameters.

Figure 2 shows the histograms of the calculated NO concentrations at equivalence ratios $\varphi = 0.76$, 1.06, and 1.54. These histograms reveal the shape of the PDFs of the NO concentrations. At each equivalence ratio, the distribution has a tail toward the high NO concentrations. This characteristic shape is in accordance with the lognormal distributions of the rate parameters for $\varphi = 0.76$ and 1.54, whereas the PDFs have two peaks for $\varphi = 1.06$. This bimodal distribution was reproduced by using other random parameter sets. We have not found an explanation to this interesting fact.

Variance of simulation results can be obtained not only by Monte Carlo but also using local uncertainty analysis (see Eq. (6)). The latter method is frequently criticized due to its local manner and linear approximation, but in our previous investigations [7–9], in all cases good agreement was found between the 1σ standard deviations obtained from local uncertainty and Monte Carlo calculations. Figure 3 shows the 1σ standard deviation of the calculated NO concentration as a percentage of the mean value. Below the stoichiometric equivalence ratio, it is in the order of 20%–40%, whereas above this threshold it is in the range of 60%–90%. The only exception is $\varphi = 0.67$ in Case I, in which the 1σ standard deviation is quite high, 50%–60% with both methods. There is always a fairly good agreement between the 1σ standard deviations calculated by the Monte Carlo and the local uncertainty analyses.

The great advantage of local uncertainty analysis is that the origin of the calculated uncertainty can be traced back to the various parameters. Partial variances $\sigma^2_{\mathrm{K}\,j}(Y_i)$ and $\sigma^2_{\mathrm{T}j}(Y_i)$, and their percentage contribution to the overall variances indicate the share of the uncertainty of parameter j to the uncertainty of result i. In

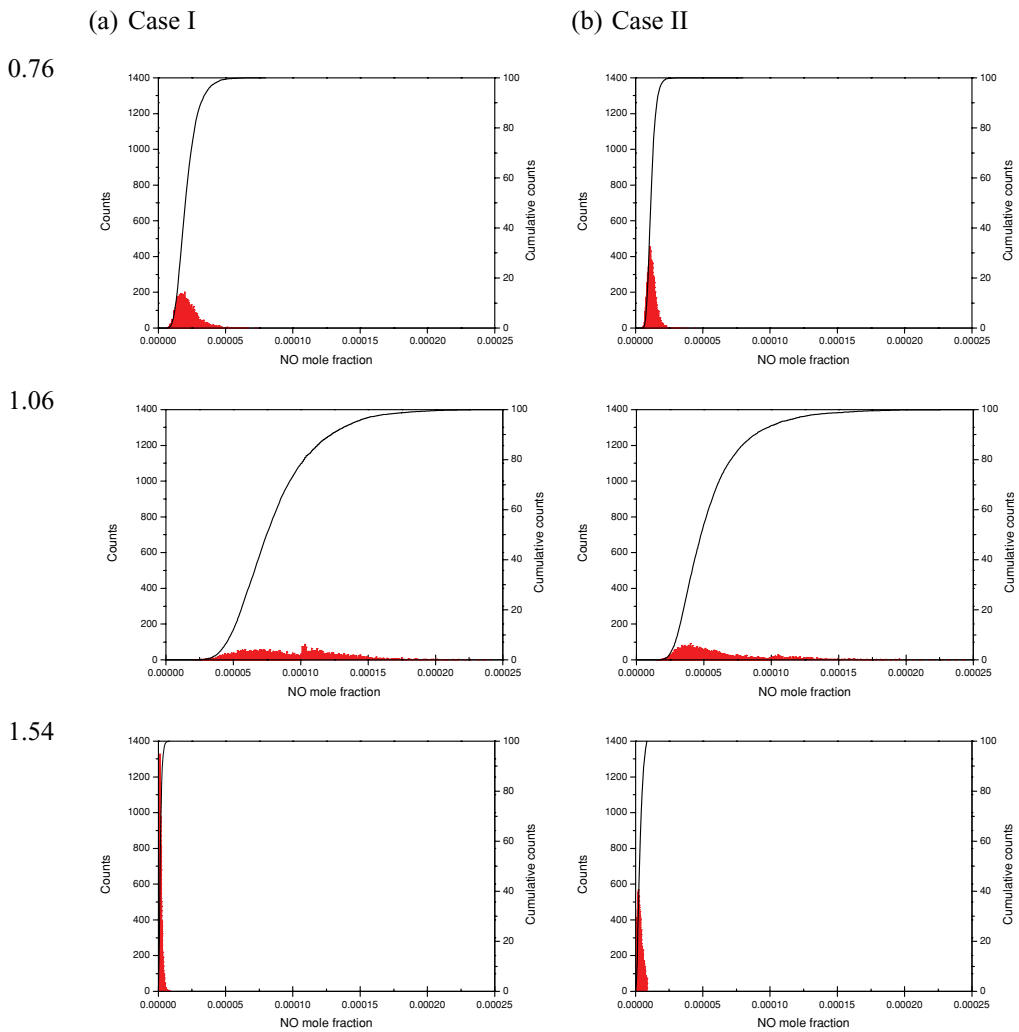

Figure 2 The approximate probability density function (PDF) and cumulative distribution function (CDF) of the calculated NO concentration at equivalence ratios $\varphi = 0.76$, 1.06, and 1.54; (a) in Case I and (b) in Case II. [Color figure can be viewed in the online issue, which is available at www.interscience.wiley.com.]

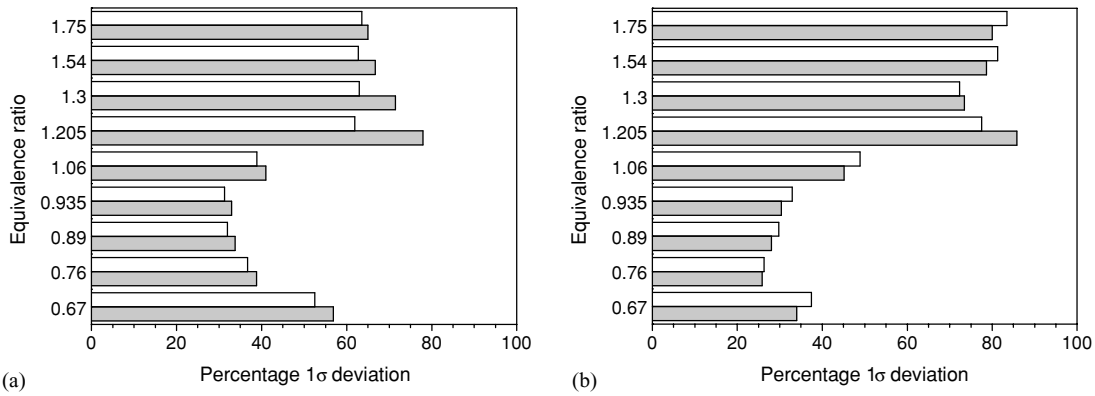

Figure 3 Comparison of the 1σ standard deviations, given as a percentage of the mean value, calculated by the Monte Carlo method (white bar) and local uncertainty analysis (gray bar); (a) in Case I and (b) in Case II.

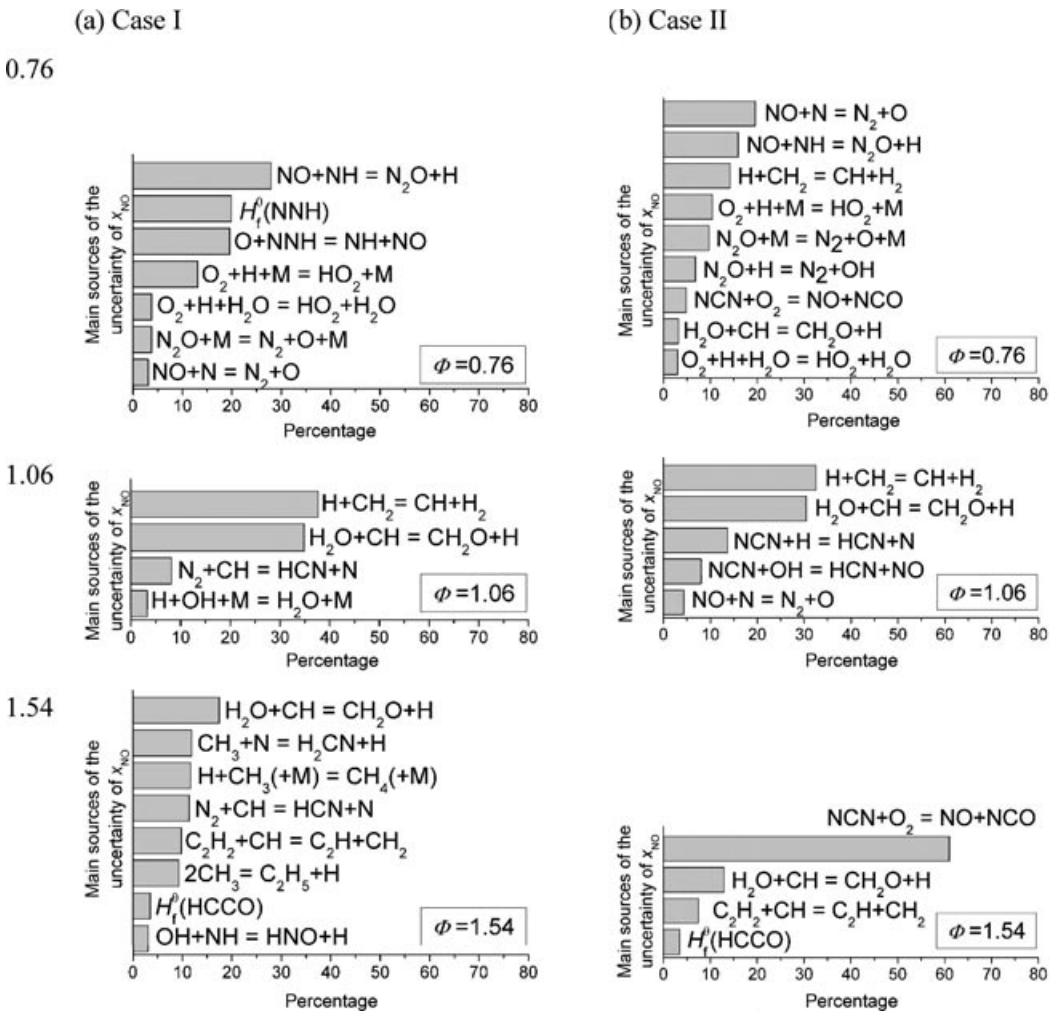

Figure 4 The main contributing rate parameters and enthalpies of formation to the uncertainty of NO concentration at equivalence ratios $\varphi = 0.76$, 1.06, and 1.54. Only contributions higher than 3% are plotted; (a) in Case I and (b) in Case II.

these simulations, there were only 4–9 parameters for each equivalence ratio that contribute to NO concentration uncertainty with more than 3%, as defined by Eq. (7). Figure 4 shows the main contributing rate parameters and enthalpies of formation to the uncertainty of NO concentration, at equivalence ratios $\varphi = 0.76$, 1.06, and 1.54 in both cases. A parameter has high uncertainty contribution, if it is an influential parameter (i.e., it has a high sensitivity coefficient) and also if the parameter value has high uncertainty.

Comparing the two cases at all equivalence ratios, there are several common sources of the uncertainty. In lean mixtures ($\varphi = 0.76$), in both cases the main sources of uncertainty are the rate parameters of reactions $NO + N = N_2 + O$, $NO + NH = N_2O + H$, $O_2 + H + M = HO_2 + M$ (together with $O_2 + H + H_2O = HO_2 + H_2O$), and $N_2O + M = N_2 + O + M$. However, in Case I the enthalpy of formation of species NNH and reaction $O + NNH = NH + NO$ appears, both correspond to the route NNH. In Case II these are present in the mechanism, but do not appear to be important. Instead, the CH and NCN reactions are highlighted, showing the increasing importance of the prompt route in this mechanism. In near stoichiometric mixtures ($\varphi = 1.06$), rate parameters of reactions $H + CH_2 = CH + H_2$ and $H_2O + CH = CH_2O + H$ have high uncertainty contribution in both cases. In Case I reaction $N_2 + CH = HCN + N$ appears, which is not present in Case II. Instead of this, two NCN reactions cause high uncertainty at this equivalence ratio in Case II: $NCN + H = HCN + N$ and $NCN + OH = HCN + NO$. In rich mixtures ($\varphi = 1.54$), the high uncertainty share belongs to

rate parameters of reactions $H_2O + CH = CH_2O + H$, $C_2H_2 + CH = C_2H + CH_2$, and enthalpy of formation of species HCCO in both cases. The important reaction $NCN + O_2 = NO + NCO$ in Case II is missing from the mechanism in Case I. Instead of this reaction, several hydrocarbon reactions and the HCN formation reaction ($N_2 + CH = HCN + N$) cause significant uncertainty of the calculated NO concentration. All in all, 20 reactions are listed in Fig. 4. This means that only a small fraction of the reaction steps cause the main part of the uncertainty of the calculated NO concentration. The uncertainty of the simulated NO concentration can be decreased, if the values of these parameters were known more precisely. The above list of reactions may be used as a guideline for planning experimental studies for the investigation of nitrogen chemistry in hydrocarbon flames.

It is clear from Fig. 4 that rate parameters have higher uncertainty contributions than the thermodynamic parameters (enthalpies of formation). The influence of the uncertainty of the thermodynamic and kinetic parameters on the uncertainty of the calculated NO concentration is contrasted in Fig. 5 by comparing the extent of the terms σ_K^2 and σ_T^2 of Eq. (7) to the overall variance $\sigma_j^2(Y_i)$. The contribution of thermodynamic parameters to the uncertainty of the results is less significant than that of the kinetic parameters, but certainly cannot be neglected. Figure 5 shows that the investigated two mechanisms behave very differently in this view. In Case I, in lean mixtures the uncertainty of NO concentration caused by the thermodynamic parameters (at least 15%) is significantly larger than it is in Case II (less than 5%). In rich mixtures, there is no significant difference between the cases, the uncertainty caused by the thermodynamic parameters is about 5%. These results can be explained by the individual contributions. At lean mixtures, the enthalpy of formation of NNH causes high uncertainty only in Case I, but the uncertainty of enthalpy of formation of HCCO is important in both cases.

As discussed in the previous section, NO can be formed during methane combustion in four ways. The contributions of these routes to the final NO concentration depend on the circumstances of the reaction. Also, in the simulations these contributions depend on the selection of parameters. In the literature, there are several papers in which the relative weight of the NO formation routes is investigated (see, e.g., [37,40,51–57]). Investigations of the various routes that are based on systematically modified mechanisms obtained by deleting one or more NO formation routes [37,52,53,55] neglect the cooperation of the reactions of the different routes. Papers dealing with the normalized local sensitivity coefficients [57] or the net reaction rates [40,51,54] of the key reactions of the routes do not commit this error, but calculations for the investigation of the various routes at the nominal parameter set could be misleading, because it may strongly depend on the actual parameter set chosen. We applied here a different approach for the estimation of the contributions of various routes. This method was based on the reaction rates of key reactions and was implemented in the Monte Carlo calculations, so the results are not limited to the nominal values of the parameters.

Since all N_2 that is consumed in reaction (R1) is finally converted to NO, the rate of thermal route was considered to be equal to the rate of reaction step (R1). The rate of the prompt route is equal to the rate of reaction step (R2) (step (R2a) for Case I and step (R2b) for Case II). We assumed that the rates of N_2O and NNH routes are equal to the sum of the rates of steps (R3)–(R6) and steps (R7)–(R12), respectively. In this approach, no assumptions are made for the rate of any reaction or for the concentration of any radical, and the

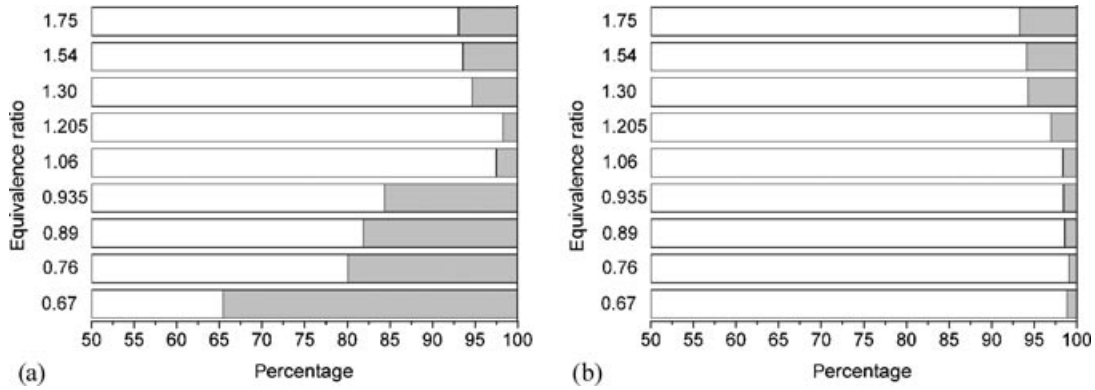

Figure 5 Share of the uncertainty caused by kinetic data (white areas) and the thermodynamic data (gray areas) at several equivalence ratios in the range $\varphi = 0.67$–1.75; (a) in Case I and (b) in Case II.

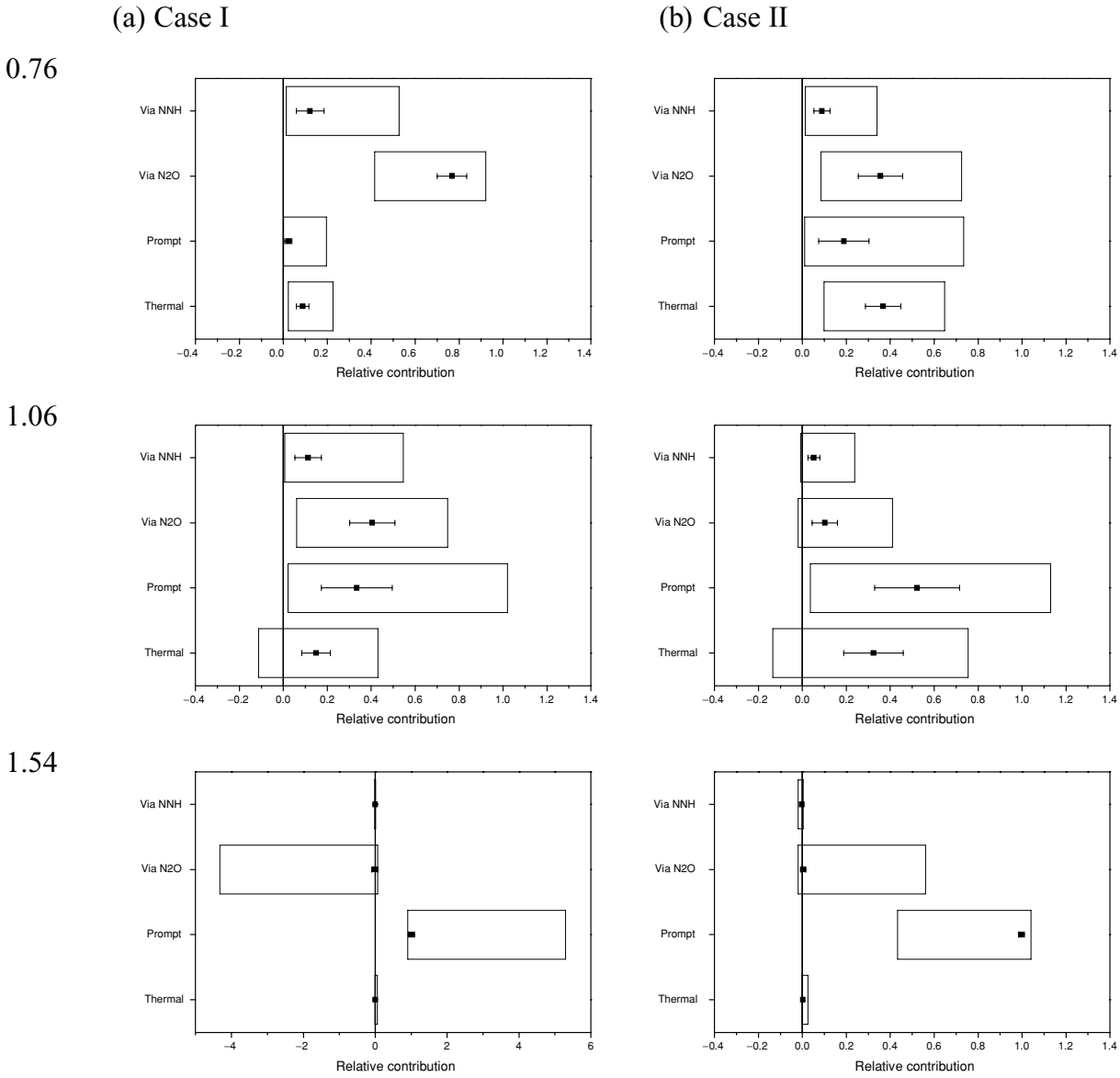

Figure 6 The relative importance of the NO formation routes at equivalence ratios $\varphi = 0.76$, 1.06, and 1.54; (a) in Case I and (b) in Case II. The symbols indicate the averages of the relative importance of the NO formation routes; the vertical lines, the 1σ error limits of the simulation data. The boxes show the achievable range by tuning all parameters simultaneously within their physically realistic limits.

reaction mechanisms were not modified. However, we have to note that the N_2O route is overpredicted in this method, because significant amount of N_2O leaves the reactor without conversion to NO.

During the Monte Carlo analysis, at each parameter set, the rates of the NO formation routes were calculated and the share of the routes was obtained. The results were analyzed by statistical methods: The average, minimal, and maximal values were determined and approximate PDFs were plotted. The results are presented in Figs. 6–8. Figure 6 presents the relative importance of the NO formation routes at $\varphi = 0.76$, 1.06, and 1.54 in both cases. Figures 7 and 8 show the distribution of the four formation routes as histograms at equivalence ratios $\varphi = 0.76$ and $\varphi = 1.06$ in Cases I and II, respectively. The histograms corresponding to $\varphi = 1.54$ are not presented, because at this equivalence ratio the prompt route is the most significant, and it would have been difficult to create a sensible graph.

At $\varphi = 0.76$ and in Case I, the main route is via N_2O, which gives almost 80% of the NO produced. In Case II, there is no such main route, but all routes

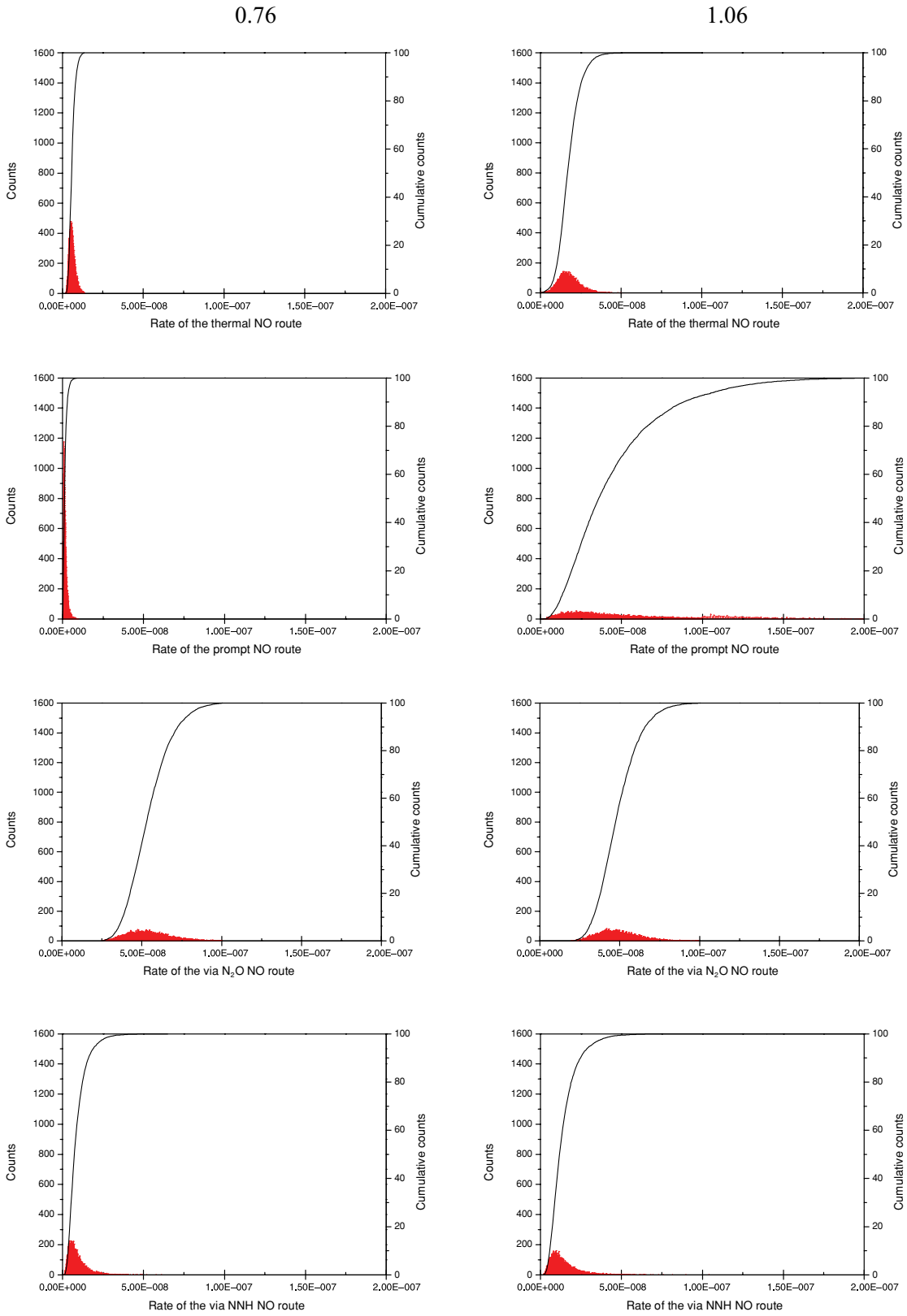

Figure 7 The approximate PDF and CDF of the rates of the four main routes leading to NO formation at equivalence ratios $\varphi = 0.76$ and 1.06 in Case I. [Color figure can be viewed in the online issue, which is available at www.interscience.wiley.com.]

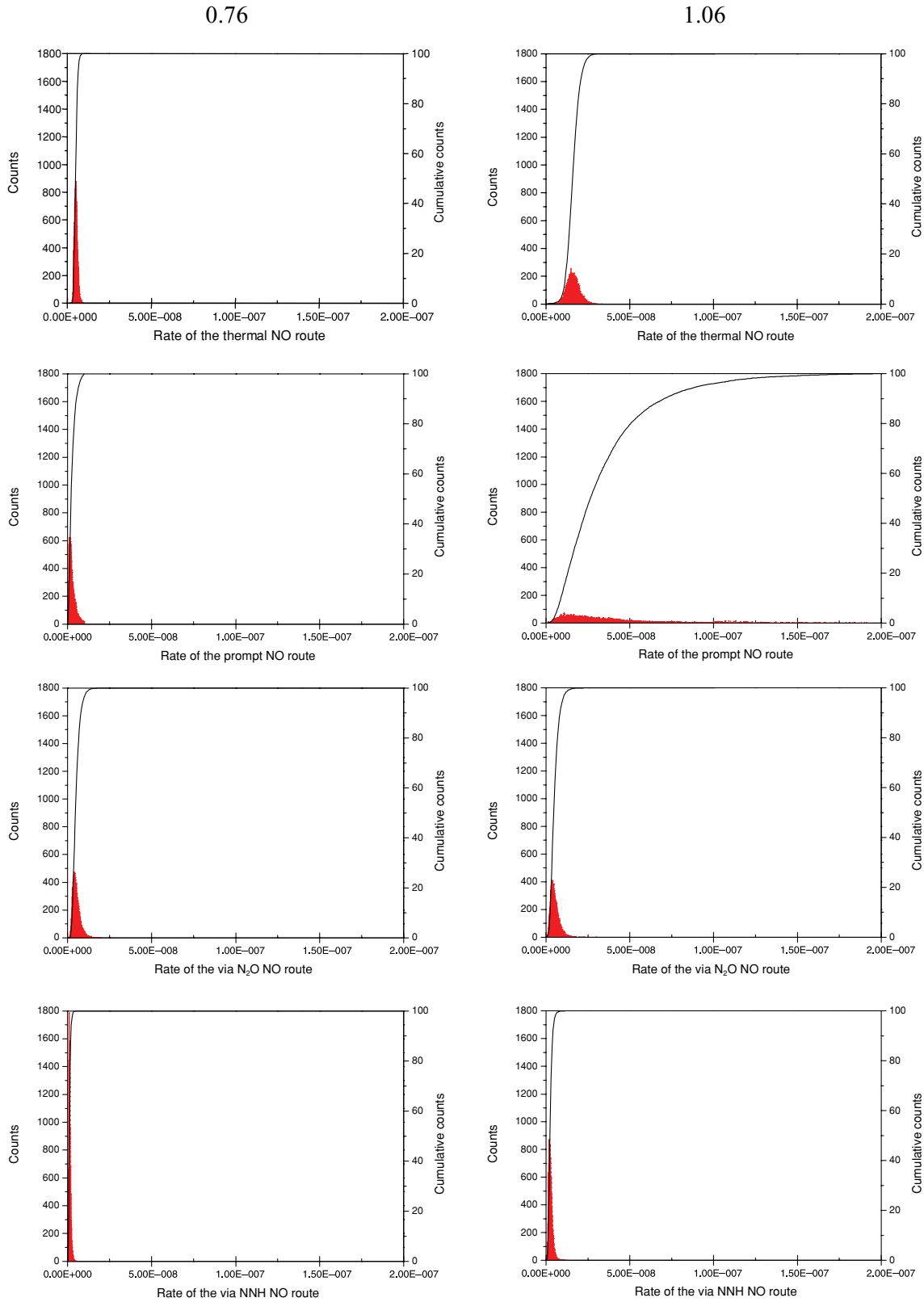

Figure 8 The approximate PDF and CDF of the rates of the four main routes leading to NO formation at equivalence ratios $\varphi = 0.76$ and 1.06 in Case II. [Color figure can be viewed in the online issue, which is available at www.interscience.wiley.com.]

contribute to the NO formation significantly. In Case I, the absolute contribution of the route through N_2O does not change when the equivalence ratio increases to 1.06, while the other routes are enhanced, especially the prompt route. This implies that the relative importance of the N_2O route is decreasing. At $\varphi = 1.54$, the prompt route is almost the unique route for the NO formation. However, it is interesting that for some parameter sets negative values appear in Fig. 6. This means that there were parameter sets that defined mechanisms in which the NO, formed in one or other routes, was partially converted back to N_2 by the key reactions of other route(s). For example, in Case I at $\varphi = 1.54$, it is possible that some NO formed by the prompt route is partially converted back to N_2 by the N_2O route initiation steps. In Case II the N_2O route is almost never a sink of NO at the same conditions. Figures 7 and 8 indicate that the prompt route has the highest uncertainty, which can be understood, because the uncertainty of the reactions of C/H species has a significant contribution to the uncertainty of NO formation via the prompt route. This uncertainty is more emphasized at higher equivalence ratios. These results on the relative contributions of the NO formation routes are generally in accordance with the general rules derived by the common textbooks, but there are some unexpected ones. For example, it was not expected that at lean and stoichiometric conditions the contribution of the various NO formation routes could vary from insignificant to dominant, depending on the values of parameters by changing these values within their realistic limits. This revealed how misleading the similar investigations limited to the nominal values of parameters could be.

CONCLUSIONS

Nitric oxide is a major air pollutant, and almost all emitted NO comes from combustion processes. The good understanding of the NO formation chemistry is very important. This includes the knowledge of the reliability of the NO concentration calculations in the simulation of perfectly stirred reactor experiments and the share of the main NO formation routes.

In this paper, two versions of the Leeds methane oxidation mechanism with the NO_x reaction block were used. In Case I, the enthalpies of formation of all species were updated to reflect the development in the accuracy of thermodynamic data since the publication [44] of the mechanism. There is an accumulating body of evidence that the major intermediate of the prompt NO formation is not HCN, as it was previously assumed, but NCN. For this reason, we created a modified version of the Leeds mechanism, called Case II mechanism, in which the debated reaction $N_2 + CH = HCN + N$ was replaced with reaction $N_2 + CH = NCN + H$. Other producing and consuming reactions of NCN were also added to the mechanism. In Case II, the rate parameters of the high sensitivity reactions of the N-species were also updated.

The present calculations confirm that simple comparison of the experimental data and the results of chemical kinetic simulations is not informative enough. For lean and stoichiometric mixtures, the experimental data of Bartok et al. [48], considering their uncertainty, are within the 1σ standard deviation of the simulation results in both cases. In Case I at the simulation of rich mixtures, no realistic tuning of the parameters could reproduce the measured NO concentrations. Inclusion of the NCN reactions (Case II) generally decreased the uncertainty of the calculated NO concentrations. In Case II at rich mixtures, the experimental points were outside the 1σ standard deviation of the simulation results, but the calculations indicated that a realistic set of rate parameters for this extended mechanism could reproduce the experimental data.

The standard deviations of the calculated NO concentrations were calculated by both local uncertainty and Monte Carlo analyses, and good agreement was found between the two methods at each equivalence ratios in both cases.

Parameters having the highest uncertainty contributions were identified. The important parameters were mainly related to reactions of NO formation routes. The lists of the important reactions in both cases are similar, but the prompt route related reactions are much more emphasized in Case II. The uncertainty of NO concentration caused by enthalpies of formations of species was smaller than those of the rate coefficients of reactions. Only the enthalpy of formation of NNH plays a significant role in lean mixtures, and only in Case I. Determination with lower uncertainty of these Arrhenius parameters, and enthalpies of formation would significantly lower the uncertainty of the calculated NO concentration. In lean mixtures, the uncertainty contributions of enthalpies of formation were much larger in Case I than in Case II. In rich mixtures, the contributions of enthalpies of formation were small and there was no significant difference between the cases.

A reaction rate-based method was introduced and applied in the Monte Carlo calculations to determine the contribution of the various NO formation routes. The results were not limited to the nominal values of the parameters and, unlike in some previous publications, untruncated mechanisms were used. In rich mixtures, the prompt route was the only significant one in both cases. In lean mixtures the Case I mechanism favored the via N_2O route, whereas using the

Case II mechanism all routes had similar share. The dependence of the relative contributions of the NO formation routes on the values of parameters was usually quite large, which showed that taking into account the relative contributions at the nominal parameter values only might lead to misinterpretations.

The unpublished review of Prof. Lajos Zalotai on the recommended values and uncertainties of the enthalpies of formation of N-containing species was utilized. The authors thank the helpful discussions on the thermodynamic data of nitrogen species with Dr. Branko Ruscic.

BIBLIOGRAPHY

1. Warnatz, J. Proc Combust Inst 1992, 24, 553–579.
2. Bromly, J. H.; Barnes, F. J.; Muris, S.; You, X.; Haynes, B. S. Combust Sci Technol 1996, 115, 259–296.
3. Brown, M. J.; Smith, D. B.; Taylor, S. C. Combust Flame 1999, 117, 652–656.
4. Turányi, T.; Zalotai, L.; Dóbé, S.; Bérces, T. Phys Chem Chem Phys 2002, 4, 2568–2578.
5. Phenix, B. D.; Dinaro, J. L.; Tatang, M. A.; Tester, J. W.; Howard, J. B.; McRae, G. J. Combust Flame 1998, 112, 132–146.
6. Reagan, M. T.; Najm, H. N.; Ghanem, R. G.; Knio, O. M. Combust Flame 2003, 132, 545–555.
7. Zádor, J.; Zsély, I. G.; Turányi, T.; Ratto, M.; Tarantola, S.; Saltelli, A. J Phys Chem A 2005, 109, 9795–9807.
8. Zádor, J.; Zsély, I. G.; Turányi, T. Reliab Eng Syst Saf 2006, 91, 1232–1240.
9. Zsély, I. G.; Zádor, J.; Turányi, T. Proc Combust Inst 2005, 30/(1), 1273–1281.
10. Tomlin, A. S. Reliab Eng Syst Saf 2006, 91, 1219–1231.
11. Ziehn, T.; Tomlin, A. S. Int J Chem Kinet 2008, 40, 742–753.
12. Warnatz, J. In Combustion Chemistry; Gardiner, W. C. (Ed.); Springer: New York, 1984; pp. 197–360.
13. Tsang, W.; Herron, J. T. J Phys Chem Ref Data 1991, 20, 609.
14. Baulch, D. L.; Cobos, C. J.; Cox, R. A.; Esser, C.; Frank, P.; Just, T.; Kerr, J. A.; Pilling, M. J.; Troe, J.; Walker, R. W.; Warnatz, J. J Phys Chem Ref Data 1992, 21, 411–734.
15. Baulch, D. L.; Cobos, C. J.; Cox, R. A.; Frank, P.; Hayman, G. D.; Just, T.; Kerr, J. A.; Murrels, T.; Pilling, M. J.; Troe, J.; Walker, R. W.; Warnatz, J. Combust Flame 1994, 98, 59–79.
16. DeMore, W. B.; Sander, S. P.; Golden, D. M.; Hampson, R. F. J.; Kurylo, M. J.; Howard, C. J.; Ravishankara, A. R.; Kolb, C. E.; Molina, M. J. Evaluation number 12, JPL publication 97-4; Jet Propulsion Laboratory, Pasadena, CA, 1997.
17. Atkinson, R.; Baulch, D. L.; Cox, R. A.; Hampson, R. F.; Kerr, J. A.; Rossi, M. J.; Troe, J. J Phys Chem Ref Data 1999, 28, 191–393.
18. Baulch, D. L.; Bowman, C. T.; Cobos, C. J.; Cox, R. A.; Just, T.; Kerr, J. A.; Pilling, M. J.; Stocker, D.; Troe, J.; Tsang, W.; Walker, R. W.; Warnatz, J. J Phys Chem Ref Data 2005, 34, 757–1397.
19. Baulch, D. L. Personal communication, 1995.
20. Stull, D. R.; Prophet, H. JANAF Thermochemical Tables, 1971, and subsequent updates.
21. McMillen, D. F.; Golden, D. M. Ann Rev Phys Chem 1982, 33, 493.
22. Burcat, A. In Combustion Chemistry; Gardiner, W. C. (Ed.); Springer: New York, 1984; pp. 455–504.
23. Gurvich, L. V.; Veyts, I. V.; Alcock, C. B. Thermodynamic Properties of Individual Substances; Hemisphere: New York, 1989.
24. Berkowitz, J.; Ellison, G. B.; Gutman, D. J Phys Chem 1994, 98, 2744.
25. Frenkel, M.; Marsch, K. N.; Wilbrit, R. C.; Kabo, G. J.; Roganov, G. N. Thermodynamics of Organic Compounds in the Gas State; Thermodynamics Research Center: College Station, TX, 1994.
26. Tsang, W. In Energetics of Organic Free Radicals; Simoes, J. A. M.; Greenberg, A.; Liebman, J. F. (Eds.); Blackie Academic and Professional: London, 1996; pp. 22–58.
27. Kerr, J. A.; Stocker, D. W. In CRC Handbook of Chemistry and Physics, 81st ed.; CRC Press: Boca Raton, FL, 2000–2001; pp. 9-51–9-74.
28. Chase, M. W. J Phys Chem Ref Data 1998, 27, I.
29. Burcat, A. Third Millennium Ideal Gas and Condensed Phase Thermochemical Database for Combustion Technion Aerospace Engineering (TAE) Report number 867, January 2001; available at ftp://ftp.technion.ac.il/pub/supported/aetdd/thermodynamics, http://garfield.chem.elte.hu/Burcat/burcat.html, accessed 2007.
30. Sander, S. P.; Friedl, R. R.; Ravishankara, A. R.; Golden, D. M.; Kolb, C. E.; Kurylo, M. J.; Huie, R. E.; Orkin, V. L.; Molina, M. J.; Moortgat, G. K.; Finlayson-Pitts, B. J. Chemical Kinetics and Photochemical Data for Use in Atmospheric Studies, evaluation number 14, JPL publication 02-25; Jet Propulsion Laboratory, Pasadena, CA, 2003.
31. Ruscic, B.; Boggs, J. E.; Burcat, A.; Császár, A. G.; Demaison, J.; Janoschek, R.; Martin, J. M. L.; Morton, M. L.; Rossi, M. J.; Stanton, J. F.; Szalay, P. G.; Westmoreland, P. R.; Zabel, F.; Bérces, T. J Phys Chem Ref Data 2005, 34, 573–656.
32. Ruscic, B.; Pinzon, R. E.; Morton, M. L.; Von Laszevski, G.; Bittner, S. J.; Nijsure, S. G.; Amin, K. A.; Minkoff, M.; Wagner, A. F. J Phys Chem A 2004, 108, 9979–9997.
33. Ruscic, B.; Pinzon, R. E.; Morton, M. L.; Srinivasan, N. K.; Su, M.; Sutherland, J. W.; Michael, J. V. J Phys Chem A 2006, 110, 6592–6601.
34. Frenklach, M.; Packard, A.; Seiler, P.; Feeley, R. Int J Chem Kinet 2004, 36, 57.
35. Feeley, R.; Seiler, P.; Packard, A.; Frenklach, M. J Phys Chem A 2004, 108, 9573–9583.
36. Saltelli, A.; Scott, M.; Chen, K. Sensitivity Analysis; Wiley: Chichester, UK, 2000.

37. Guo, H.; Smallwood, G. J.; Fengshan, L.; Ju, Y.; Gülder, Ö. L. Proc Combust Inst 2005, 30, 303–311.
38. Moskaleva, L. V.; Lin, M. C. Proc Combust Inst 2000, 28, 2393–2401.
39. Smith, G. P. Chem Phys Lett 2003, 367, 541–548.
40. El Bakali, A.; Pillier, L.; Desgroux, P.; Lefort, B.; Gasnot, L.; Pauwels, J. F.; da Costa, I. Fuel 2006, 85, 896–909.
41. Vasudevan, V.; Hanson, R. K.; Bowman, C. T.; Golden, D. M.; Davidson, D. F. J Phys Chem A 2007, 111, 11818–11830.
42. Harding, L. B.; Klippenstein, S. J.; Miller, J. A. J Phys Chem A 2008, 112, 522–532.
43. Hughes, K. J.; Turányi, T.; Clague, A. R.; Pilling, M. J. Int J Chem Kinet 2001, 33, 513–538.
44. Hughes, K. J.; Tomlin, A. S.; Hampartsoumian, E.; Nimmo, W.; Zsély, I. G.; Ujvári, M.; Turányi, T.; Clague, A. R.; Pilling, M. J. Combust Flame 2001, 124, 573–589.
45. Glarborg, P.; Kee, R. J.; Grcar, J. F.; Miller, J. A. PSR: A Fortran Program for Modeling Well-Stirred Reactors; SAND86-8209, 1986.
46. Kee, R. J.; Rupley, F. M.; Miller, J. A. Chemkin-II: A Fortran Chemical Kinetics Package for the Analysis of Gas Phase Chemical Kinetics; SAND89-8009B, 1989.
47. Turányi, T.; Zsély, I. G. KINALC: A CHEMKIN based program for kinetic analysis, available at http:/garfield.chem.elte.hu/Combustion/Combustion.html, accessed 2007.
48. Bartok, W.; Engelman, V. S.; Goldstein, R.; del Valle, E. G. AIChE Symp 1972, 126, 30–38.
49. Bowman, C. T.; Hanson, R. K.; Davidson, D. F.; Gardiner, W. C.; Lissianski, V.; Smith, G. P.; Golden, D. M.; Frenklach, M.; Goldenberg, M. GRI-Mech 2.11, available at http://www.me.berkeley.edu/gri_mech/, accessed 2007.
50. Smith, G. P.; Golden, D. M.; Frenklach, M.; Moriary, N. W.; Eiteneer, B.; Goldenberg, M.; Bowman, C. T.; Hanson, R. K.; Song, S.; Gardiner, W. C.; lissianski, V. V.; Qin, Z. GRI-Mech 3.0, available at http://www.me.berkeley.edu/gri_mech/, accessed 2007.
51. Rortveit, G. J.; Hustad, J. E.; Li, S. C.; Williams, F. A. Combust Flame 2002, 130, 48–61.
52. Nishioka, M.; Nakagawa, S.; Ishikawa, Y.; Takeno, T. Combust Flame 1994, 98, 127–138.
53. Miller, J. A.; Bowman, C. T. Prog Energy Combust Sci 1989, 15, 287–338.
54. Naha, S.; Aggarwal, S. K. Combust Flame 2004, 139, 90–105.
55. Guo, H.; Smallwood, G. J. In 4th Mediterranean Combustion Symposium, Lisbon, Portugal, 2005, pp. VII/7.
56. Löffler, G.; Sieber, R.; Harasek, M.; Hofbauer, H.; Hauss, R.; Landauf, J. Fuel 2006, 85, 513–523.
57. Konnov, A. A. Combust Flame 2003, 134, 421–424.
58. Ruscic, B.; Boggs, J. E.; Burcat, A. J Phys Chem Ref Data 2005, 34, 573.
59. Lin, M. C.; He, Y. S.; Melius, C. F. Int J Chem Kinet 1992, 24, 498–516.
60. Tsang, W. J. Phys Chem Ref Data 1992, 21, 753–791.
61. Glarborg, P.; Alzueta, M. U.; Dam-Johansen, K.; Miller, J. A. Combust Flame 1998, 115, 1–27.
62. Davidson, D. F.; Hanson, R. K. Proc Combust Inst 1991, 23, 267.